Eur. Phys. J. D **30**, 81–92 (2004)
DOI: 10.1140/epjd/e2004-00075-5

THE EUROPEAN PHYSICAL JOURNAL D

# Numerical study of plasma-wall transition using an Eulerian Vlasov code

M. Shoucri[1], A. Cardinali[2,a], J.P. Matte[3], and R. Spigler[4]

[1] Institut de recherche d'Hydro-Québec, Varennes (Québec) J3X 1S1, Canada
[2] Associazione Euratom-ENEA sulla Fusione, Centro Ricerche Frascati, C.P. 65, 00044 Frascati, Rome, Italy
[3] INRS Énergie et Matériaux, Université du Québec, Varennes (Québec) J3X 1S2, Canada
[4] Università di Roma III, Dipartimento di Matematica, Roma, Italy

Received 27 June 2003 / Received in final form 16 October 2003
Published online 26 May 2004 

**Abstract.** A one-dimensional Eulerian Vlasov code is used to study the self-consistent solution of a plasma facing a floating collector, in the absence of an external magnetic field. Both electrons and ions are treated with a kinetic equation. A Bhatnagar-Gross-Krook (BGK) collision term is used to describe the collisions. Acceleration of the ion flow at the Debye sheath entrance is observed together with the formation of a stable steep negative electric field in front of the floating collector. This negative electric field acts to accelerate the positive ions towards the plate, pushing back the negative electrons, such that at steady state the total current collected at the plate is zero. The codes are run for a sufficiently long time on the ions time scale to ensure the ions (argon) distribution function is reaching a steady state. For the different parameters used, the solution shows the existence of persistent regular oscillations of constant amplitude when the electron collisions are very small or negligible. These oscillations will be studied. The increase in the electron collisions damps these oscillations and helps the system reach an equilibrium.

**PACS.** 52.65.Ff Fokker-Planck and Vlasov equation

## 1 Introduction

Many problems of plasma-wall interaction require a self-consistent solution of a plasma layer in contact with a wall. In industrial plasmas, these problems are important for plasma etching and ion sputtering which are at the core of a revolution in microprocessors technology and other material processing applications. The knowledge of the exact form of energy distributions of charged particles near the metal substrates immersed into the plasma, and the analyses of the changes in these distributions during the transport through both the presheath and the sheath for various biases and substrates geometries is of fundamental importance to control these processes. Probes characteristics are also of fundamental importance in industrial plasmas as well as in other plasmas applications such as tokamaks. The plasma limiter and plasma-divertor interaction are the most important problems in the edge physics of tokamaks.

There is an abundant literature which studies plasma-wall transition problems with the assumption that the electrons density can be calculated from a Boltzmann relation ([1] and references therein), and more recently the Boltzmann relation for electrons has been used in codes where the ions kinetic has been studied using a fully kinetic Vlasov equation [2,3]. Close to the wall, however, in the presence of electric fields, the electrons distribution function is non-Maxwellian and electrons should be described by a kinetic equation, since the electrons kinetic and distribution determine the rate at which a multitude of electron driven processes will proceed in low temperature plasmas. The electron energy distribution function is of fundamental importance in gas discharges since the excitation and ionization of gas atoms is, to a large part, caused by electrons. On the other hand simulations with particle in cell (PIC) codes have been used [4,5], but they suffer from high noise levels which makes it difficult to obtain accurate distribution functions and the related moments from them. Recently, an Eulerian Vlasov code [6,7] in which the electrons were treated using a kinetic equation was used to study the problem of a magnetized sheath. Eulerian Vlasov codes have very low noise level, and allow accurate calculations of the distribution functions and the macroscopic quantities associated with them. Eulerian Vlasov codes have been also recently applied for accurate solution of the problem of radio frequency (RF) inductive coupling in an argon plasma, using real electron to ion mass ratio [8]. It is the purpose of the present work to present a one-dimensional kinetic Vlasov code to study the self-consistent solution of a plasma facing a floating collector, in the absence of an external magnetic field. Both electrons and ions are treated with a kinetic equation. Two cases will be studied. First a BGK

[a] e-mail: cardinali@frascati.enea.it

term is used to describe the ion collisions and ionization, similar to the one used in reference [2], neglecting electrons collisions. Then, the effect of the electron collisions will be introduced.

The results for exact electron to ion mass ratio $m_e/m_i$ using argon and for different parameters show for very weak or negligible electron collisions the presence of steady state oscillations, and a stable steep density profile and electric field facing the floating collector plate, where strong acceleration of the ions takes place. This steady state is reached when the total current to the plate is zero. The steady state oscillations damp when the electron collisions are increased.

## 2 The pertinent equations

We study the transition of a plasma to a perfectly absorbing wall, in the absence of an external magnetic field. The phase-space is two-dimensional $x$, $\nu_x$, where the coordinates are normal to the wall. The electrons and ions distribution functions $f_e$ and $f_i$ are calculated from their respective Vlasov equation, with a BGK term included which have a collision frequency $\nu_{i,e}$

$$\frac{\partial f_{i,e}}{\partial t} + \nu_x \frac{\partial f_{i,e}}{\partial x} \pm \frac{e}{m_{i,e}} E_x \frac{\partial f_{i,e}}{\partial \nu_x} = \nu_{i,e} \left( f_{Mi,e} - f_{i,e} \right) \quad (1)$$

where $f_{Mi,e}$ is the equilibrium Maxwellian distribution for the ions or electrons. The system is closed by Poisson's equation:

$$\frac{\partial^2 \phi}{\partial x^2} = -\frac{e}{\varepsilon_0} \left( n_i(x,t) - n_e(x,t) \right) \quad (2)$$

with the electric field $E_x = -\partial\phi/\partial x$, and

$$n_{e,i}(x,t) = \int_{-\infty}^{\infty} f_{e,i}\left(x, \nu_x, t\right) d\nu_x. \quad (3)$$

The BGK collision operator (on the right hand side of Eq. (1)) in a weakly ionized plasma represents the collisions of ions (electrons) with neutral atoms. The negative term $-\nu_{i,e} f_{i,e}$ represents the rate at which ions are removed, and the positive term $\nu_{i,e} f_{Mi,e}$ is the rate of production of new ions. A similar collision term has been recently used in reference [2].

We assume an initial neutral plasma with uniform electron $n_e$ and ion $n_i$ densities such that $n_e = n_i$. We assume the initial values of the electrons and ions distribution functions to be Maxwellian, with temperature respectively of $T_e$ and $T_i$. We take our domain of integration to be $L = 150$ Debye lengths ($\lambda_{De} = \nu_{the}/\omega_{pe}$ where $\nu_{the} = \left(\kappa T_e/m_e\right)^{1/2}$, and $\omega_{pe}$ is the plasma frequency). The floating wall or absorbing plate is located at $x = 0$. We assume that the plasma extends at the right boundary, so that the point next to the boundary point is identical to the boundary point. The ions and the electrons with $\nu_x > 0$ at the right boundary are left free to leave the plasma, and the ions and electrons with $\nu_x < 0$ are assumed to enter from an identical plasma extending to the right at the next grid point, i.e. we assume $f_{i,e}\left(L + \Delta x, t\right) = f_{i,e}\left(L, t\right)$. This establishes the flux at the right boundary without forcing the distribution function at the right boundary. The exact balance between this flow at the right boundary, the charge collected at the left boundary by the floating plate is calculated as follows. At the left boundary, particles with $\nu_x < 0$ are hitting the plate, lost from the system, and collected through the current delivered at the plate (there is no incoming particles from wall at $x = 0$ since there is no particles reflected or emitted at the wall with $\nu_x > 0$):

$$\left.\frac{\partial E_x}{\partial t}\right)_{x=0} = \left.-\frac{J_x}{\varepsilon_0}\right)_{x=0} = \left.-\frac{J_{x_i} - J_{x_e}}{\varepsilon_0}\right)_{x=0} \quad (4)$$

from which:

$$\left.E_x)_{x=0} = -\frac{1}{\varepsilon_0} \int_0^t dt J_x\right)_{x=0} \quad (5)$$

$$J_{x_{e,i}})_{x=0} = \int_{-\infty}^{0} \nu_x f_{e,i}\left(0, \nu_x, t\right) d\nu_x \quad (6)$$

(only particles with $\nu_x < 0$ are hitting the wall at the left boundary and are absorbed by the wall).

We can also write:

$$\left.E_x)_{x=0} = -\frac{\partial \phi}{\partial x}\right)_{x=0} \quad (7)$$

which determines one of the boundary conditions for the solution of the potential in equation (2) at $x = 0$. For the right boundary condition on the potential, we integrate the equation:

$$\frac{\partial E_x}{\partial x} = \frac{e}{\varepsilon_0} \left( n_i - n_e \right) = \frac{\rho}{\varepsilon_0} \quad (8)$$

over the domain; we get:

$$E_x)_{x=L} - E_x)_{x=0} = \int_0^L \frac{\rho}{\varepsilon_0} dx = \frac{\sigma}{\varepsilon_0}. \quad (9)$$

The system is initially neutral $n_e = n_i$. The total charge $\sigma$ which appears in the system, in the course of the simulation, must be equal to the difference in the electric fields at the boundaries.

$E_x)_{x=0}$ is calculated from equation (5), which defines the derivative of the potential at $x = 0$. Since the derivative of the potential is specified at the left boundary, we can fix the potential to be zero at the right boundary (if $\phi$ is a solution, $\phi + const$ is also a solution). The resulting electric field $E_x)_{x=L}$ calculated at $x = L$ from the solution of Poisson's equation must satisfy equation (9), which

is used as a check. The agreement between $E_x)_{x=L}$ calculated from the Poisson's equation and the value calculated from equation (9):

$$E_x)_{x=L} = \frac{\sigma}{\varepsilon_0} + E_x)_{x=0} \tag{10}$$

was fairly good. So equation (10) is used as a check.

Equation (10) gives the exact balance between the charge collected at the plate at the left boundary, the charge appearing in the plasma during the simulation, and the electric field at the right boundary, in a system which is only initially neutral, and evolves to a steady non-neutral state. The fairly good agreement obtained in verifying equation (10) necessitated a sufficiently fine grid in space to calculate the total charge $\sigma$ accurately at every time step, and a sufficiently small time step $\Delta t$ to calculate the accumulation of charge at the plate at $x = 0$ from equation (5).

The Vlasov equations in equation (1) were solved by a method of fractional steps associated with cubic splines interpolation as discussed in references [9,10], and as successfully applied recently for the study of RF inductive coupling in argon plasmas [8]. The maximum velocity for each species extended to four initial thermal velocity for the species considered $\left(\nu_{\max_{ei}} = 4\nu_{th_{e,i}}\right)$, 70 grid points were used for the ion species in the velocity domain $[-\nu_{\max_i}; +\nu_{\max_i}]$, and 200 grid points for the electrons in the velocity domain $[-\nu_{\max_e}; +\nu_{\max_e}]$. 300 or 400 grid points were used in space to discretize the spatial domain $[0; L]$. The fractional steps scheme, when centered in space and time, is second order. To advance equation (1) for a time step $\Delta t$, we apply the following fractional steps:

- step 1: solve for $\Delta t/2$

$$\frac{\partial f_{i,e}}{\partial t} + \nu_x \frac{\partial f_{i,e}}{\partial x} = 0$$

- update the electric field from equation (2);
- step 2: solve for $\Delta t/2$

$$\frac{\partial f_{i,e}}{\partial t} \pm \frac{e}{m_{i,e}} E_x \frac{\partial f_{i,e}}{\partial \nu_x} = 0;$$

- step 3: solve for $\Delta t$

$$\frac{\partial f_{i,e}}{\partial t} = \nu_{i,e} \left( f_{M_{i,e}} - f_{i,e} \right).$$

  This equation is solved using a simple Eulerian scheme, since we usually use a sufficiently small $\Delta t$.
- step 4: repeat step 2;
- step 5: repeat step 1.

The solution of the equations in steps 1, 2, 4, and 5 are calculated using cubic splines interpolation as discussed in references [8–10].

Argon plasma is considered. In Section 3, we present the results for the case where the electron collisions are neglected. In Section 4, the effect of the electron collisions on the results of Section 3 will be presented.

## 3 Results for the case where electron collisions are neglected

The results will be presented using normalized units. Unless otherwise stated in the graphical output, time is normalized to the ion plasma period $\omega_{pi}^{-1}$ for argon, velocity is normalized to $c_s = \sqrt{\kappa T_e/m_i}$, and length is normalized to the Debye length $\lambda_{De} = c_s \omega_{pi}^{-1}$. We present results for an argon plasma, with $m_e/m_i = 1/(40 \times 1836)$, and with $T_e/T_i = 2$. Real mass ratio is used in the calculation. We start the system from an initially uniform plasma with $n_e = n_i = 1$. Electrons are followed on the electron plasma period time scale, which in our normalized units is given by $\omega_{pe}^{-1}/\omega_{pi}^{-1} = 1/(40 \times 1836)^{1/2} = 0.0037$. We choose a time-step $\Delta t_i = 0.001$ for the ions. For the electrons, the time-step $\Delta t_e = \Delta t_i/10 = 0.0001$. As discussed for equation (10), we choose this small time-step to ensure the different charges calculated in equation (10) are accurately calculated.

This means that we integrate the electrons for 10 time-steps with $\Delta t_e$ (updating the electric field), while keeping the ions fixed. Then the argon ions are advanced with $\Delta t_i$. With $\Delta t_e = 1 \times 10^{-4}$, the electrons were integrated about 37 times during an electron plasma period (given by 0.0037 as mentioned above). Although a bigger time-step could have been chosen for the ions, this computational effort was taken in view of the different oscillations appearing in the present case in the system in space and time and the rapid evolution at the beginning, and to ensure equation (10) is accurately satisfied during the entire simulation. $N = 300$ grid points were used in space for this simulation. Note that a simulation effected by increasing the time-step by a factor of 2 for the ions reproduced exactly the same results. In the present simulation we use for the argon collision frequency a ratio $\nu_i/\omega_{pi} = 0.05$, and $\nu_e = 0$.

We ran the code for sufficiently long time up to $\omega_{pi}t = 150$ to ensure the ions distribution function has reached its steady state. Also pushing the calculations further in time was reproducing the same steady state. The system appeared reaching its steady state well before $\omega_{pi}t = 100$. Until the end of the simulation, a constant and regular oscillation of the potential, of a period close to 0.024 (around 6 electron plasma periods) is present and repeating itself very regularly. At the end of the simulation at $\omega_{pi}t = 150$, several thousand of these oscillations have been performed, verifying equation (10) with the same accuracy, and without showing any sign of attenuation. Figure 1 shows the contour plot of the argon ions distribution function, with a smooth transition from a distribution very close to Maxwellian at the right boundary, to a distribution showing a strong acceleration toward the negative velocities in the Debye sheath near the plate. Cuts in the contour plot at: (a) $x = 0$; (b) $x = 5\lambda_{De}$; (c) $x = 15\lambda_{De}$; (d) $x = 75\lambda_{De}$; (e) $x = 150\lambda_{De}$; are presented in the bottom of Figure 1, showing at $x = 0$ and at $x = 5\lambda_{De}$ the strong shift of the distribution functions toward the negative velocities in the sheath region. In our normalized units where time is normalized to $\omega_{pi}^{-1}$, the argon

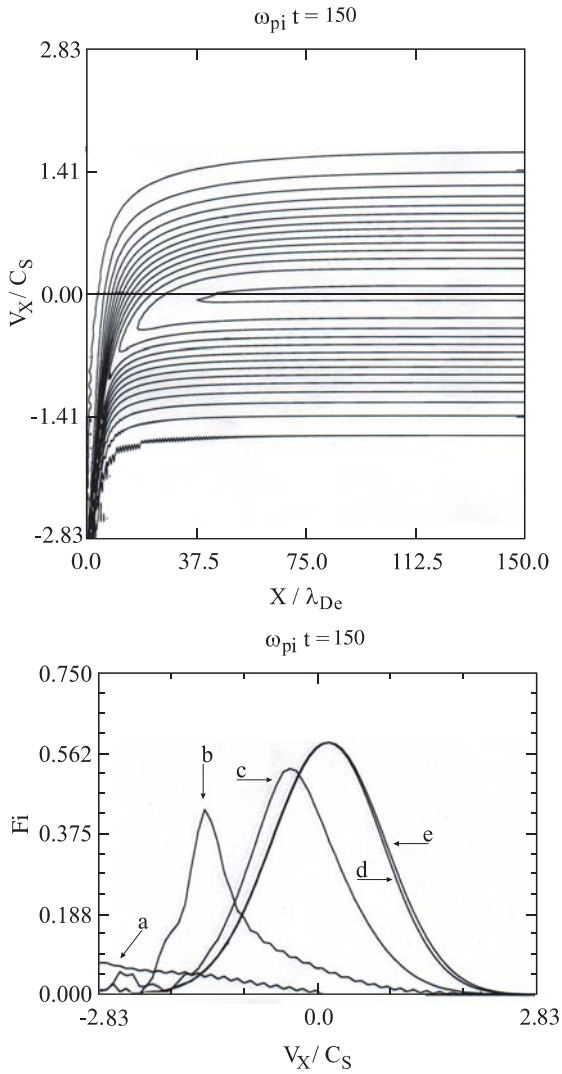


**Fig. 1.** Contour plot of the distribution functions for the argon ions at $\omega_{pi}t = 150.0$. Case without electron collisions. Lower curves, distribution function obtained by cuts at: (a) $x = 0$; (b) $x = 5\lambda_{De}$; (c) $x = 15\lambda_{De}$; (d) $x = 75\lambda_{De}$; (e) $x = 150\lambda_{De}$ ($\nu_i/\omega_{pi} = 0.05$).

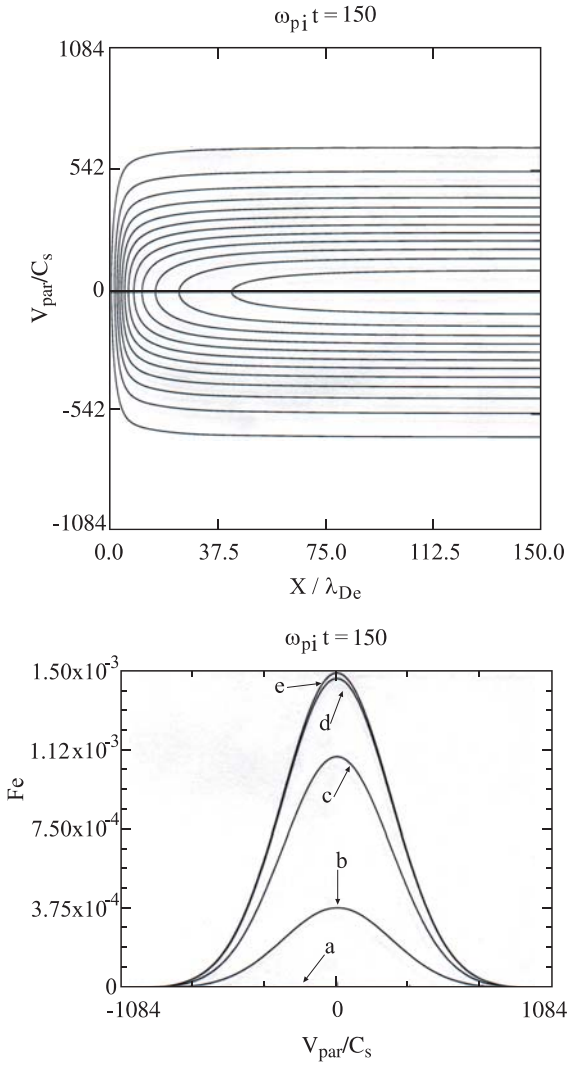


**Fig. 2.** Same as Figure 1, but for the electron distribution function at $\omega_{pi}t = 150.0$.

plasma period is $2\pi = 6.28$. Figure 2 shows the electron distribution function at $\omega_{pi}t = 150$. We show in Figure 3 the potential over half a period of potential oscillation, at $t = 150$ and $t = 150.012$. During this oscillation, the slope of the potential at the origin $x = 0$ is remaining essentially constant, fixed by the value of the charge collected at the floating plate, determined by equations (5) and (7). This value of the charge collected at the floating plate determines also from equation (7) the value of the electric field at $x = 0$, shown in Figure 4 to be fixed and equal to about $-1.375$. The electric field is shown in Figure 4 at the peak ($\omega_{pi}t = 150.0$) and minimum ($\omega_{pi}t = 150.012$) of the potential in Figure 3. During the oscillation, the electric field in Figure 4 shows a steady steep negative profile in a layer of few Debye lengths where the ions are strongly accelerated towards the plate, and the electrons strongly repelled from the plate. Note in the flat part of

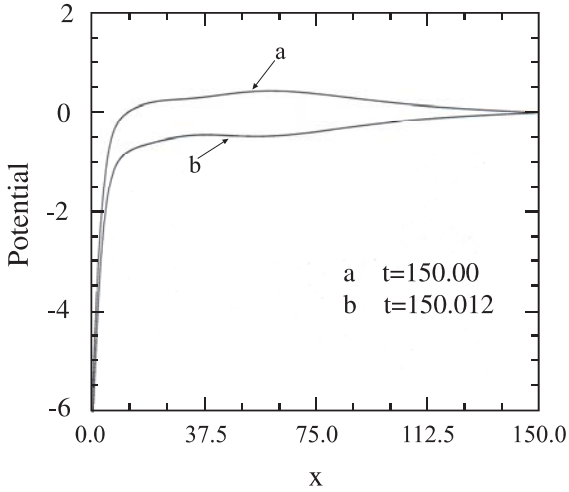


**Fig. 3.** Potential during a period of oscillation, from $\omega_{pi}t = 150.0$ until $\omega_{pi}t = 150.012$ ($\nu_i/\omega_{pi} = 0.05$).

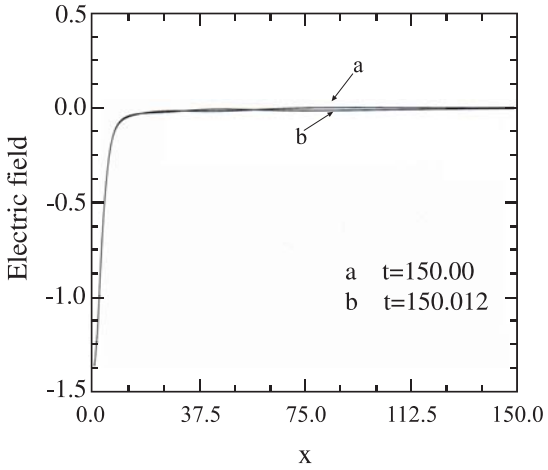


**Fig. 4.** Electric field at $\omega_{pi}t = 150.0$ and $\omega_{pi}t = 150.012$ ($\nu_i/\omega_{pi} = 0.05$).

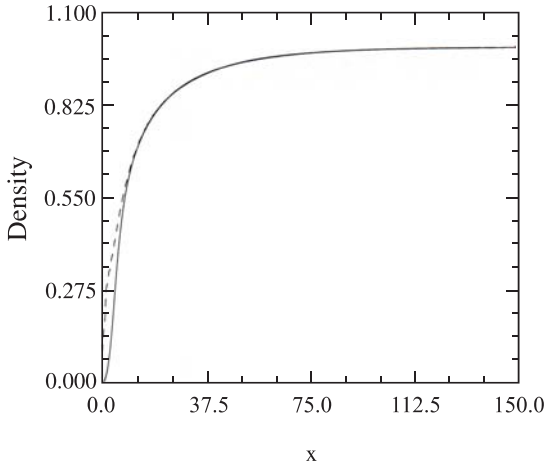


**Fig. 5.** Density at $\omega_{pi}t = 150.0$ (full curves for electrons, dotted curve for argon ions, $\nu_i/\omega_{pi} = 0.05$).

the profile a small oscillations around zero. Figure 5 shows the density profile in which the ions show a finite value at the plate, but the electrons show a steep profile with an almost vanishing density at the plate (full curves). The density profile of the argon ions (broken curve) in Figure 5 is essentially constant. The density profile of the electrons (full curve) oscillates and the points of intersection of the electron density curves behave essentially as nodes points during the oscillations, and the electrons density at these points is constant. (This point will be discussed in more details for the results with $\nu_i/\omega_{pi} = 0.1$ where the oscillations increase). The charge $n_i - n_e$ at $t = 150$ and 150.012 (at the peak and minimum of the potential oscillation) is shown in Figure 6. Note the decline in front of the plate. There is a very small oscillation, apparent especially on the flat part of the charge profile, from which results the oscillation of the potential in Figure 3. Figure 7 shows the argon current $J_{x_i}$ (full curve) and the argon velocity $J_{x_i}/n_i$ (broken curve). The heavy ions show no oscillations, reaching the plate at a constant small current. The electron currents $J_{x_e}$ in Figure 8 (full curves) are showing

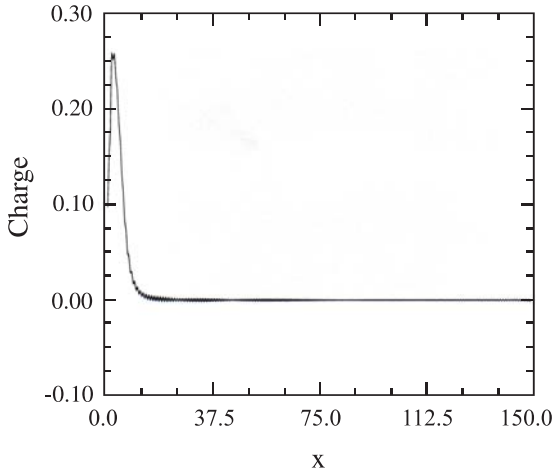


**Fig. 6.** Charge $n_i - n_e$ at $\omega_{pi}t = 150.0$ and $\omega_{pi}t = 150.012$ ($\nu_i/\omega_{pi} = 0.05$).

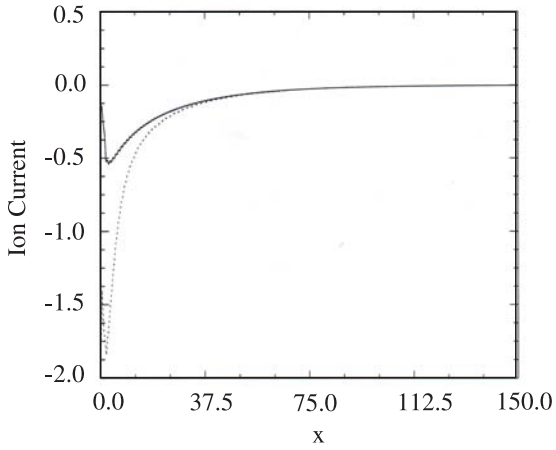


**Fig. 7.** Argon ions current $J_{x_i}$ (full curve) and velocity $J_{x_i}/n_i$ (broken curve) at $\omega_{pi}t = 150.0$, and $\omega_{pi}t = 150.012$ ($\nu_i/\omega_{pi} = 0.05$).

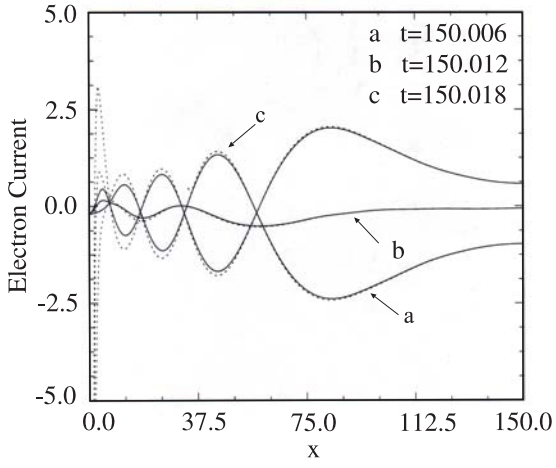


**Fig. 8.** Electrons current $J_{x_e}$ (full curve) and velocity $J_{x_e}/n_e$ (broken curve) at $\omega_{pi}t = 150.006$, $\omega_{pi}t = 150.012$ and $\omega_{pi}t = 150.018$ ($\nu_i/\omega_{pi} = 0.05$).

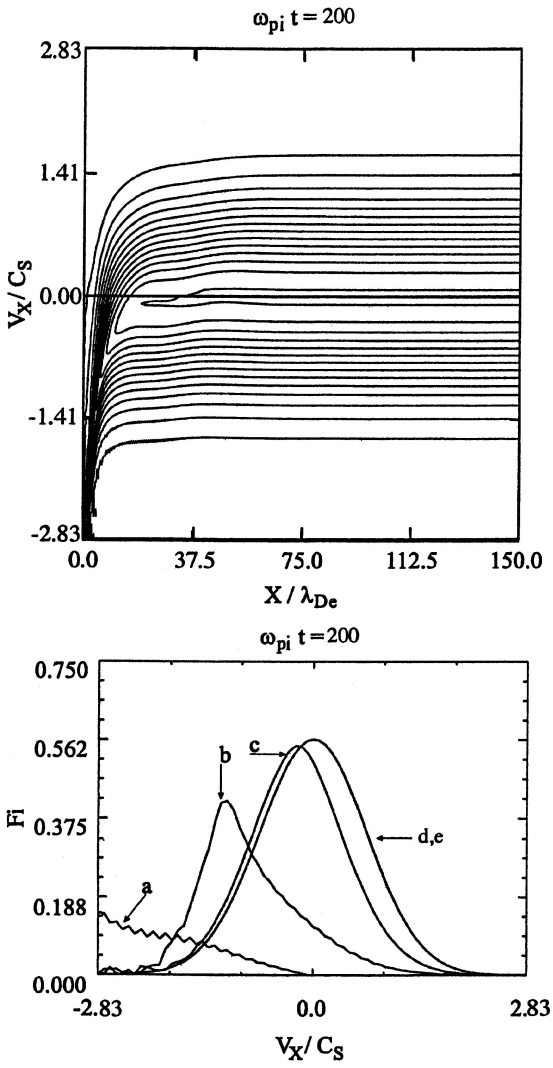


**Fig. 9.** Contour plot of the distribution functions for the argon ions at $\omega_{pi}t = 200.0$. Case without electron collisions. Lower curves, distribution function obtained by cuts at: (a) $x = 0$; (b) $x = 5\lambda_{De}$; (c) $x = 15\lambda_{De}$; (d) $x = 75\lambda_{De}$; (e) $x = 150\lambda_{De}$ ($\nu_i/\omega_{pi} = 0.1$).

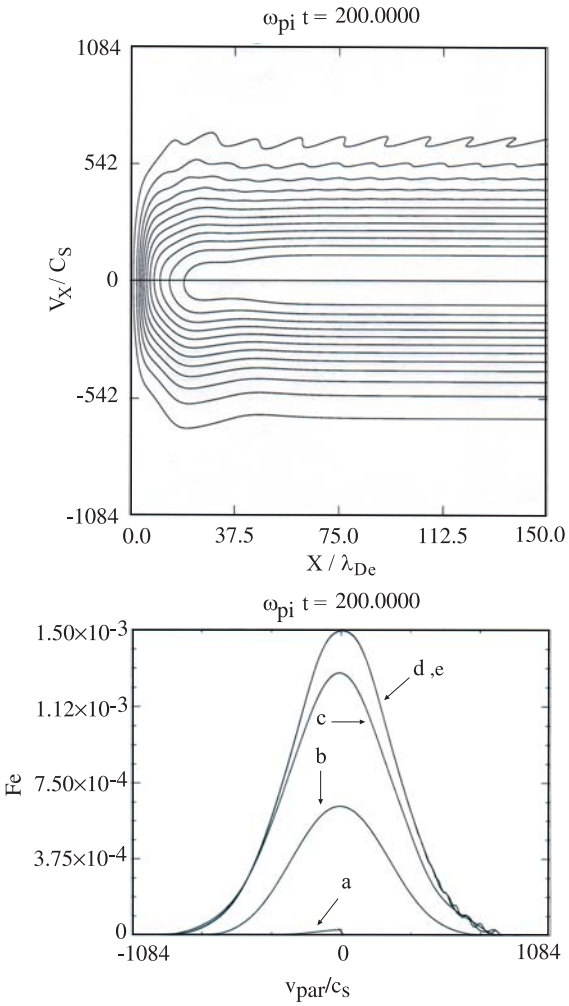


**Fig. 10.** Same as Figure 9, but for the distribution function of the electrons at $\omega_{pi}t = 200.0$ ($\nu_i/\omega_{pi} = 0.1$).

a more important oscillation, reaching the plate at the left at essentially the same current as the ions, ensuring that $J_x = J_{x_i} - J_{x_e}$ is zero at the plate ($x = 0$) in the steady state phase. Note the oscillation which persisted with a regular period of 0.024 for several thousands oscillations. Hence the steady state we see is a state in which the total current to the plate is essentially zero, and the electric field at the plate remains essentially constant and equal to about $-1.375$ as apparent in Figure 4. (This discussion on the edge electric field and charge holds for the simulations with $\nu_i/\omega_{pi} = 0.1$ still to be presented).

We present another set of results with $\nu_i/\omega_{pi} = 0.1$ and $\nu_e = 0$, all other parameters remaining identical. This simulation was done with $\Delta t = 5 \times 10^{-4}$, and using 400 grid-points in space. For the electrons, the time-step was $5 \times 10^{-5}$, so the ions are advanced in time every once, every 10 time-step for the electrons. Figure 9 presents at $\omega_{pi}t = 200.01$ the argon distribution function for this case, which seems to be at steady state, and is distorted and accelerated in a thinner layer than the corresponding one in Figure 1 for $\nu_i/\omega_{pi} = 0.05$ (since the driving collision term to the equilibrium distribution is stronger than for the results presented in Fig. 1). In Figures 10 and 11, the contour plot of the electrons show a sawtooth structure in space. The distortion and oscillation of the potential in Figure 12 are shown during a half period of oscillation, from $\omega_{pi}t = 200.0$ until $\omega_{pi}t = 200.011$. The amplitude of the oscillations are more important and show a period of 0.022, slightly lower than the period we see in the first simulation (at $\nu_i/\omega_{pi} = 0.05$). (Note in Fig. 12 at the end of the period the curve g at $\omega_{pi}t = 200.22$ essentially identical to the curve a at $\omega_{pi}t = 200.0$.) For the present set of parameters, the variation of the ions collision frequency shows a small effect on the observed period of oscillation. The regular period of the sawtooth structure in Figures 10 and 11 reflects exactly the regular period of the potential in Figure 12. The negative electric field in front of the plate in Figure 13 is pushing back the electrons. However immediately behind this steady negative

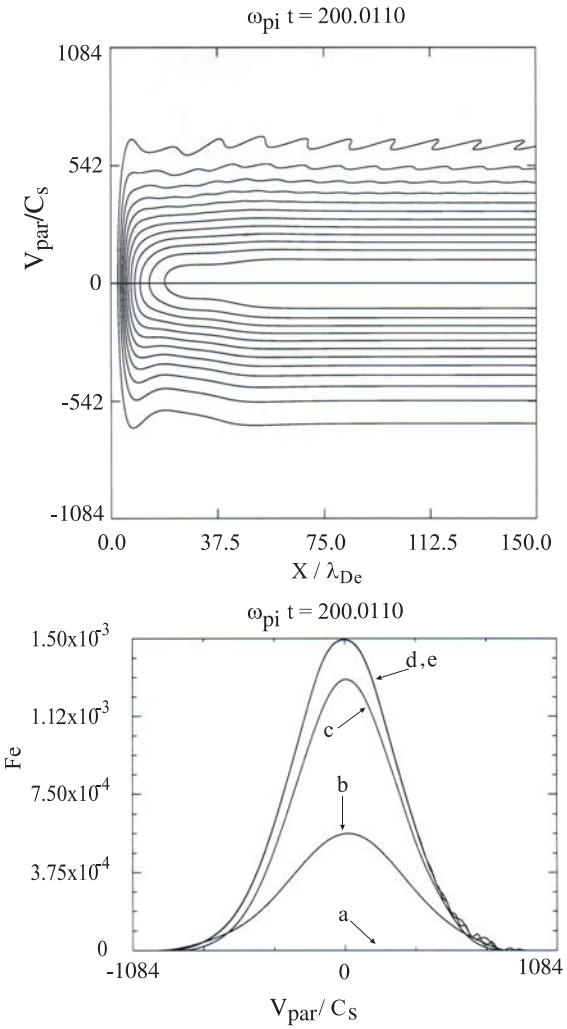


**Fig. 11.** Same as Figure 9, for the distribution function of the electrons at $\omega_{pi}t = 200.011$ ($\nu_i/\omega_{pi} = 0.1$).

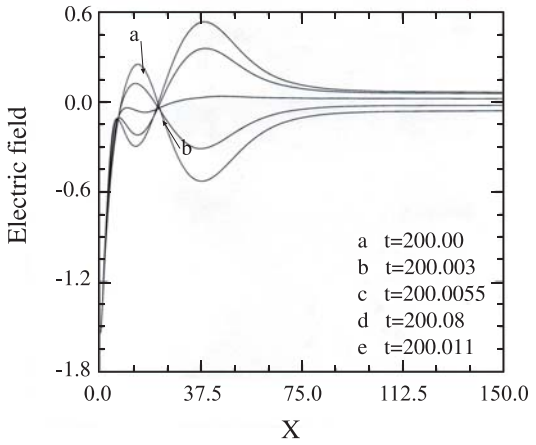


**Fig. 13.** Electric field during a half period from $\omega_{pi}t = 200.0$ until $\omega_{pi}t = 200.011$ ($\nu_i/\omega_{pi} = 0.1$).

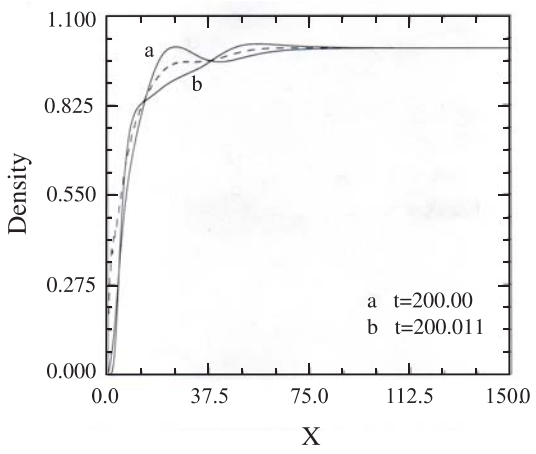


**Fig. 14.** Density profiles for electrons (full curve) and argon ions (broken curve), at $\omega_{pi}t = 200.0$, and $\omega_{pi}t = 200.011$ ($\nu_i/\omega_{pi} = 0.1$).

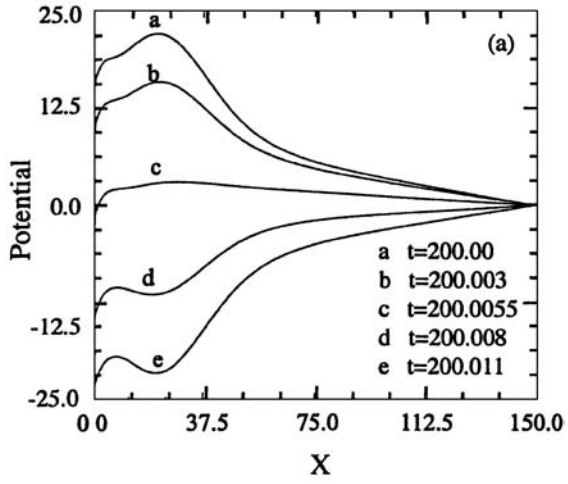


**Fig. 12.** Potential during a half period of oscillation, from $\omega_{pi}t = 200.0$ until $\omega_{pi}t = 200.011$; the period extends until $\omega_{pi}t = 200.022$ ($\nu_i/\omega_{pi} = 0.1$).

field, there is an oscillating electric field. Electrons arriving with negative velocities from the right boundary can be decelerated when the oscillating electric field is negative, or accelerated when the field is positive, resulting in a bunching or modulation of the same period as the oscillation. The reflected electrons traveling to the right with positive velocities show the effect of this modulation or bunching with this sawtooth structure. As we can judge from the last two top contours in Figures 10 and 11, the higher the velocity, the longer the length of a sawtooth period. If we take the sawtooth at the last contour on the top, the length period is about 15 Debye lengths. The velocity, normalized to $(T_e/m_i)^{1/2}$ as in the calculations, it is about 640. So the period of one of the sawtooth is about $15/640 \approx 0.022$. Figure 12 shows the spatial profiles evolution during a half-period of 0.011. The density in Figure 14 is shown at the peak and minimum of the potential in Figure 12. Note in Figure 13 a higher electric field at the plate, equal to about –1.51, and equal to the charge collected at the floating plate as given by equation (5), as previously discussed. In Figure 14, the density of argon

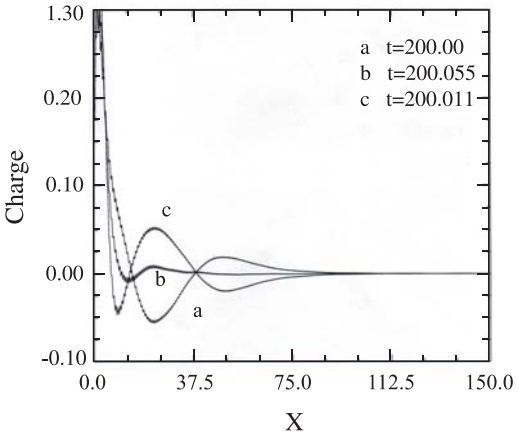


**Fig. 15.** Charge $n_i - n_e$ at $\omega_{pi}t = 200.0$, $\omega_{pi}t = 200.0055$ and $\omega_{pi}t = 200.011$ ($\nu_i/\omega_{pi} = 0.1$).

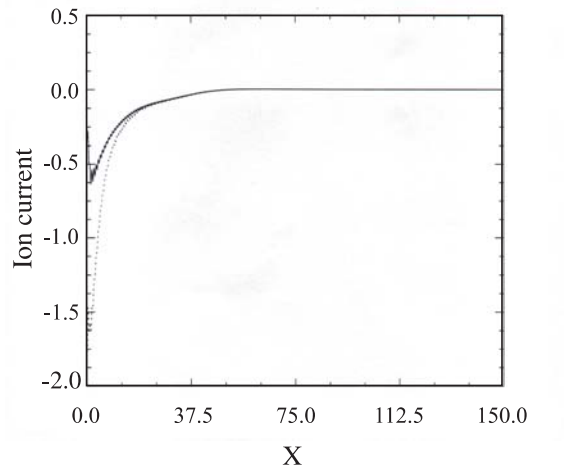


**Fig. 16.** Argon ions current $J_{x_i}$ (full curve) and velocity $J_{x_i}/n_i$ (broken curve), at $\omega_{pi}t = 200.00$ and $\omega_{pi}t = 200.011$ ($\nu_i/\omega_{pi} = 0.1$).

at the plate is higher, the argon density profile (broken curve) is essentially constant, while the electron density profiles (solid curves) show a modulation around the argon density curve, which translates into nodes (points of constant density) appearing along $x$. This modulation appears also in the charge $n_i - n_e$ in Figure 15. Note the charge in the few Debye lengths layer close to the plate remaining essentially constant. Note also the oscillations of the electric field $E_x)_{x=L}$ at $x = L$ in Figure 13 reflecting exactly the oscillation of the total charge $\sigma$, since $E_x)_{x=0}$ is equation (10) is constant as we can verify at the left boundary.

Figure 16 gives the ion current $J_{x_i}$ (full curve), and the velocity $J_{x_i}/n_i$ (both essentially constant in time). Note the ion current at the plate about twice that in Figure 7, while the velocity peak (broken curve) is slightly lower. Figure 17 gives the electrons current, showing a more important oscillation. These oscillations repeated themselves with the same period 0.022 several thousand times. The electron $J_{x_e}$ at the plate $x = 0$ is such that the total current $J_x = J_{x_i} - J_{x_e}$ at the plate $x = 0$ is equal to zero. To

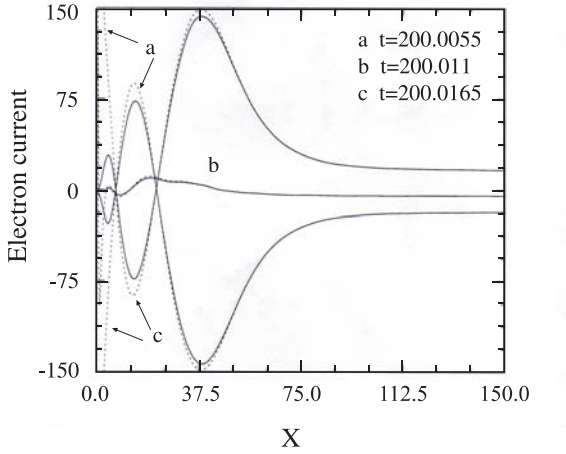


**Fig. 17.** Electrons current $J_{x_e}$(full curve) and velocity $J_{x_e}/n_e$ (broken curve) at $\omega_{pi}t = 200.0055$, $\omega_{pi}t = 200.011$, and $\omega_{pi}t = 200.0165$ ($\nu_i/\omega_{pi} = 0.1$).

conclude this section, for a variation of $\nu_i/\omega_{pi}$ from 0.05 to 0.1, and for the parameters we are choosing, we get a thinner layer of acceleration of the argon ions close to the plate together with higher ion and electron currents and density at the plate, and a stronger modulation of the electron density charge, and electron current in space. At steady state, the total current collected at the plate is zero, and the potential and electric field profiles in front of the plate are constant.

## 4 Results for the case including electron collisions

We repeat the simulation presented in Section 3 for $\nu_i/\omega_{pi} = 0.1$, by including in equation (1) an electron collision term with $\nu_e/\omega_{pi} = 0.1$, or $\nu_e/\omega_{pe} = 0.1\sqrt{m_e/m_i}$. Figures 18–24 present the results obtained in this case, which show essentially the same features as discussed in Section 3. However the electron oscillations as discussed in the previous section are more damped. Figure 18 shows the electron distribution function, with the sawteeth structure appearing in the contour plot, as previously discussed. The amplitude of the electron oscillations as apparent in Figure 19 for the potential are more damped compared to those presented in Figure 12. Similarly in Figure 20 for the electric field, in Figure 21 for the density profiles, in Figure 22 for the charge, and in Figure 24 for the electron current. It should a period of oscillations of 0.0235. The results in Figure 23 for the argon ions current $J_{xi}$ show essentially the same steady state current profile as in Figure 16. Again the steady state shows the total current $J_{xi} - J_{xe}$ at $x = 0$ at the left plate equal to zero.

We next increase the electron collision frequency to $\nu_e/\omega_{pi} = 0.3$, or $\nu_e/\omega_{pe} = 0.3\sqrt{m_e/m_i}$. Figures 25–29 present the results. We reach rapidly in this case a state-state without oscillations. Figure 25 shows the contour plot of the electron distribution function. Figure 26

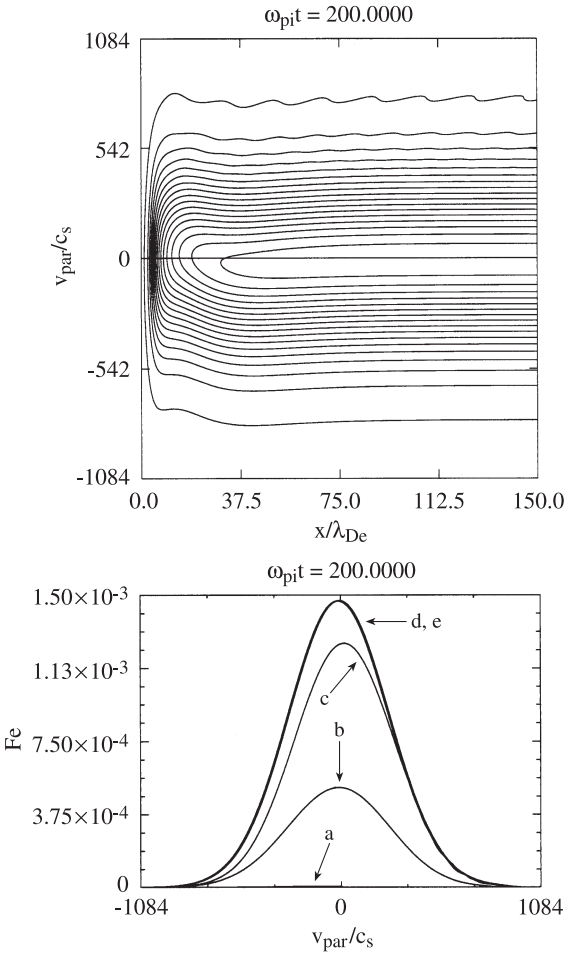


**Fig. 18.** Same as Figure 11, but for the electron distribution function at $\omega_{pi}t = 200$.

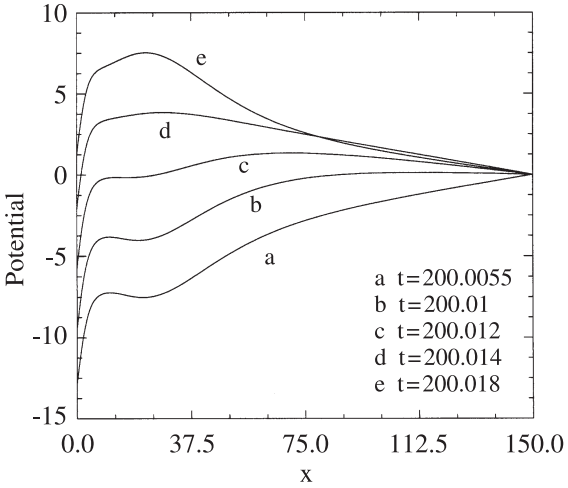


**Fig. 19.** Potential during a half period of oscillation, $\omega_{pi}t = 200.0055$ to $\omega_{pi}t = 200.018$; the period is extended until $\omega_{pi}t = 200.029$ ($\nu_e/\omega_{pi} = 0.1$).

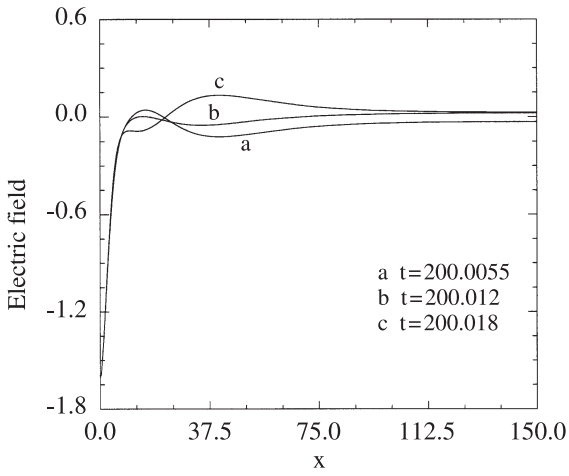


**Fig. 20.** Electric field during half period from $\omega_{pi}t = 200.0055$ to $\omega_{pi}t = 200.018$; ($\nu_e/\omega_{pi} = 0.1$).

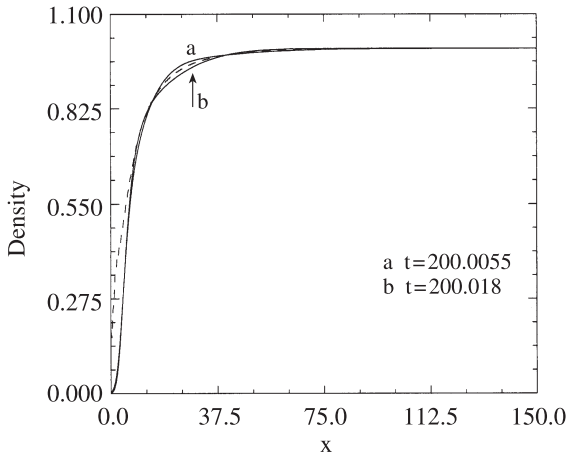


**Fig. 21.** Density profiles for electrons (full curve) and argon ions (broken curve), at $\omega_{pi}t = 200.0055$ and $\omega_{pi}t = 200.018$ ($\nu_e/\omega_{pi} = 0.1$).

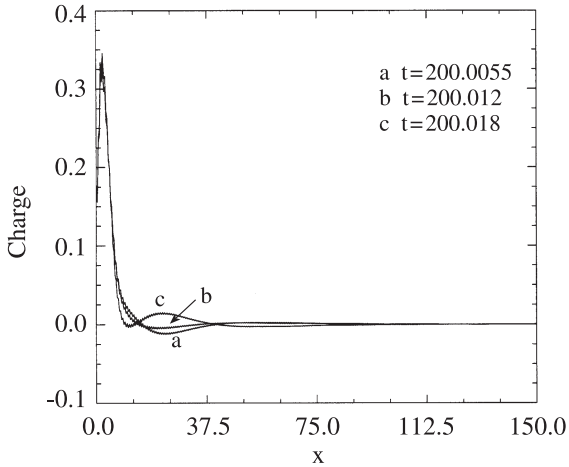


**Fig. 22.** Charge $n_i - n_e$ at $\omega_{pi}t = 200.0055$, $\omega_{pi}t = 200.012$; and $\omega_{pi}t = 200.018$ ($\nu_e/\omega_{pi} = 0.1$).

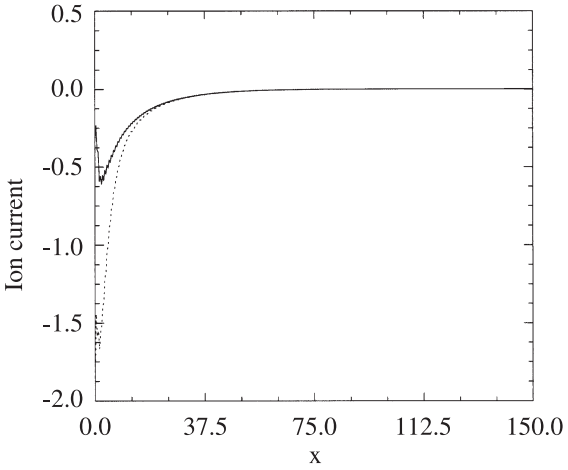


**Fig. 23.** Argon ions current $J_{xi}$ (full curve) and velocity $J_{xi}/n_i$ (broken curve) at $\omega_{pi}t = 200.0055$ ($\nu_e/\omega_{pi} = 0.1$).

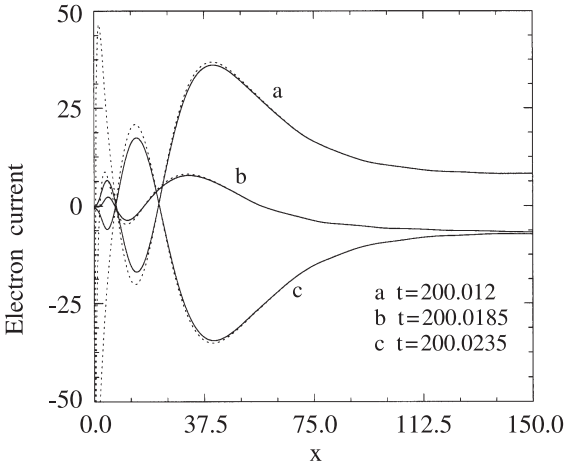


**Fig. 24.** Electrons current $J_{xe}$ (full curve) and velocity $J_{xe}/n_e$ (broken curve) at $\omega_{pi}t = 200.012$, $\omega_{pi}t = 200.0185$ and $\omega_{pi}t = 200.0235$ ($\nu_e/\omega_{pi} = 0.1$).

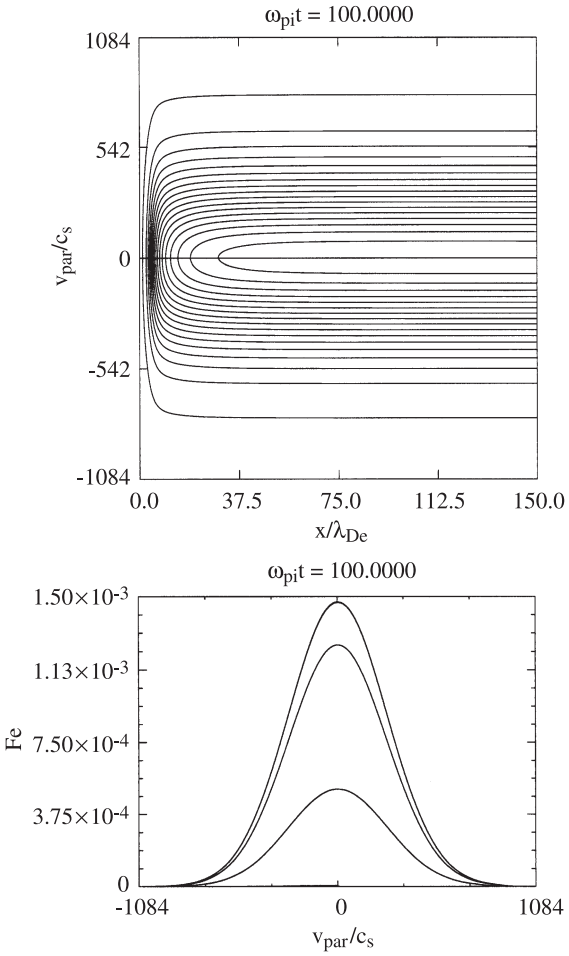


**Fig. 25.** Contour plot of the distribution functions of the electrons for the case $\nu_e/\omega_{pi} = 0.3$. Lower curves, distribution functions obtained by cuts at: (a) $x = 0$; (b) $x = 5\lambda_{De}$; (c) $x = 15\lambda_{De}$; (d) $x = 75\lambda_{De}$; (e) $x = 150\lambda_{De}$.

presents the potential (full curve) and the electric field (broken curve). The charge collected at the plate as in equation (5), which is equal to the electric field at $x = 0$ in Figure 26, is $-1.61758$. The charge $\sigma$ appearing in the system is 1.61818. The resulting electric field at $x = L$, as defined by equation (10), is $E_x)_{x=L} = -1.61758 + 1.61818 = 0.0006$. The density profile is given in Figure 27 (solid line for the electrons, broken line for the ions). Figure 28 presents the equilibrium charge $(n_i - n_e)$. In Figure 29, we present the electron current in full curve, the ion current in broken curve, which are reaching the plate at $x = 0$ with the same value. The total current (dotted curve in Fig. 29) is exactly equal to zero at the plate at $x = 0$.

## 5 Conclusions

The effect of the electron distribution function on the plasma parameters of an argon discharge has been the subject of important studies, using a volume-averaged global

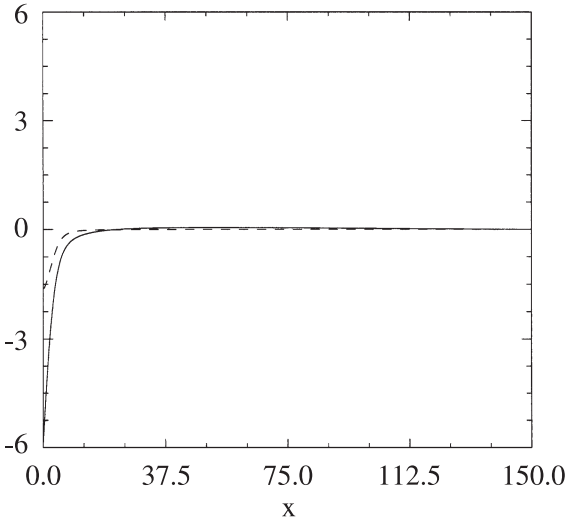


**Fig. 26.** Potential (full curve) and electric field (broken curve) for the case $\nu_e/\omega_{pi} = 0.3$.

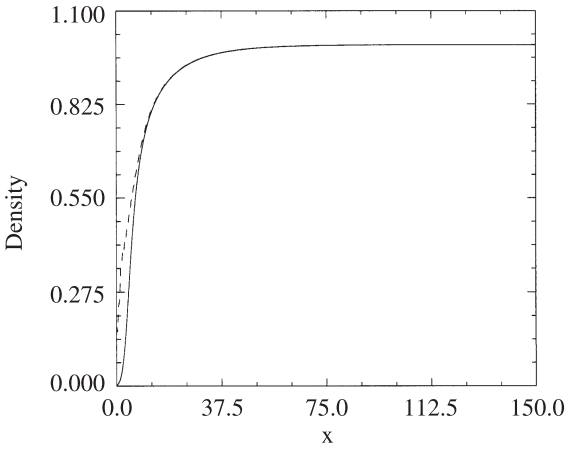


**Fig. 27.** Density profiles for electrons (full curve) and argon ions (broken curve), for the case $\nu_e/\omega_{pi} = 0.3$.

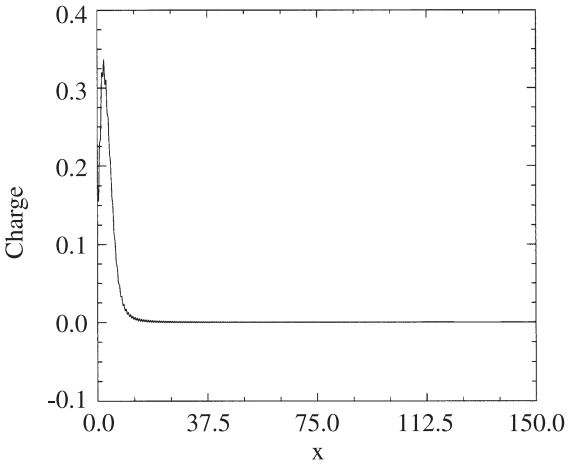


**Fig. 28.** Charge $n_i - n_e$ for the case $\nu_e/\omega_{pi} = 0.3$.

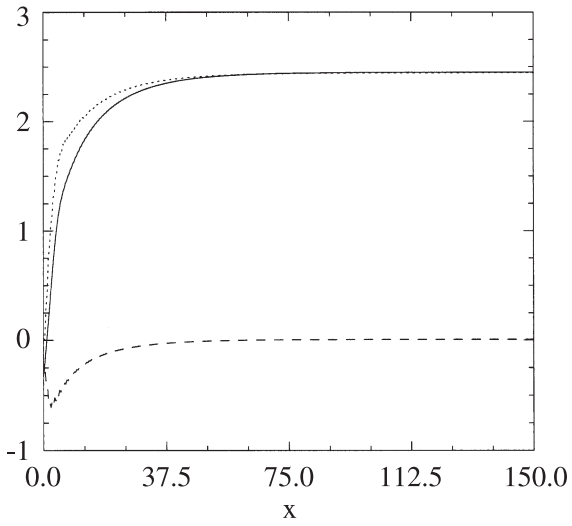


**Fig. 29.** Electron current (full curve), ion current (broken curve), and total current (dotted curve), for the case $\nu_e/\omega_{pi} = 0.3$.

model, which is not meant to give accurate values of the plasma parameters, but rather some indication on how one parameter depends on another ([15] and references therein). In the present work however, we have presented a one-dimensional Eulerian Vlasov code, in which both electrons and ions are treated with a kinetic equation, to study the self-consistent solution of a plasma facing a floating collector. Accurate calculation of the distribution functions have been presented. In the first case a collision term has been used for the positive ion species only, modelling collisions and ionization, hence a steady state can be reached for the ions. The electrons are allowed to flow from the right boundary and established a sheath structure with steady state oscillations. A constant charge and electric field is established at the left plate, accelerating the ions toward the left plate and decelerating the electrons such that the total current at the left plate is zero. Adding the electron collisions has a tendency to damp and eliminate the electron oscillations. In all cases, charges appearing in the system, or collected a the plate at $x = 0$ are accurately taken care of, and the agreement in verifying equation (10) is fairly good. The codes are run for a sufficiently long time to ensure the distribution functions are reaching a steady state or equilibrium. The inclusion of the electrons kinetic is important since the electrons distribution function determines the rates at which a multitude of electron driven processes will proceed in low temperature plasmas. When oscillations are present, we have followed the electron oscillations appearing for several thousand periods, for the different cases considered. They always remained regular in their periodicity, and especially for $\nu_i/\omega_{pi} = 0.1$ they showed in the density plots what appears to be nodes at which the electron density remained constant during the oscillations. So the picture of the density oscillations in space in this case is essentially that of a standing wave. The case with argon ions we have studied showed the ions strongly accelerating towards the floating plate by a steep electric field in front of the plate, accelerating the ions and pushing back the electrons. The inclusion of a self-consistent treatment for the generation and loss processes (namely ionization, attachment, detachment, recombination), can be done as reported in reference [16], and can certainly have important effects on the observed oscillations of the electrons. A self-consistent collision and source term operators will allow to study more accurately the smooth transition from the neutral plasma bulk to the formation of a charge separation, an electric field and the acceleration of the ions in the Debye sheath in front of the floating plate.

M. Shoucri is grateful to Gruppo Nazionale per la Fisica Matematica for a financial support of one month which made this work possible, and for the hospitality of Dr. F. Romanelli at the Plasma Physics Division of the ENEA at Frascati.

## References


1. R. Stangeby, *The Plasma Boundary of Magnetic Fusion* (Institute of Physics Publishing, Abingdon (UK), devices, 2000)
2. F. Valsaque, G. Manfredi, J. Nucl. Mater. **290**, 763 (2001)
3. H. Gerhauser, H.A. Claassen, Contr. Plasma Phys. **38**, 331 (1998)
4. R. Chodura, Phys. Fluids **25**, 1628 (1982)
5. D. Tskhakaya, S. Kuhn, *Proc. EPS Conf.*, Madeira, Portugal, 2001
6. M. Shoucri, K.H. Finken, *Proc. EPS Conf.*, Madeira, Portugal, 2001; N. Schupfer, S. Kuhn, M. Shoucri, *Proc. EPS Conf.*, Madeira, Portugal, 2001
7. M. Shoucri, H. Gerhauser, K.H. Finken, Czech. J. Phys. **52**, 1121 (2002)
8. M. Shoucri, J.P. Matte, A. Cote, J. Phys. D **36**, 2083 (2003)
9. C.Z. Cheng, G. Knorr, J. Comp. Phys. **22**, 330 (1976)
10. M. Shoucri, R. Gagne, J. Comp. Phys. **24**, 445 (1997); J. Comp. Phys. **27**, 315 (1978)
11. T.H. Chung, L. Meng, H.J. Yoon, J.K. Lee, Jap. J. Appl. Phys. **36**, 2874 (1997)
12. R.N. Franklin, J. Snell, J. Phys. D: Appl. Phys. **31**, 2532 (1998)
13. I.G. Kouznetsov, A.J. Lichtenberg, M.A. Lieberman, J. Appl. Phys. **86**, 4142 (1999)
14. R. Hrach, Czech. J. Phys. **49**, 155 (1999)
15. J.T. Gudmundsson, Plasma Sources Sci. Technol. **10**, 76 (2001)
16. O.V. Batischchev, M. Shoucri, A. Batischcheva, I.P. Shkarofsky, J. Plasma Phys. **61**, 347 (1999)